

TRAVELING EDGE STATES IN MASSIVE DIRAC EQUATIONS ALONG SLOWLY VARYING EDGES

PIPI HU, PENG XIE, AND YI ZHU

ABSTRACT. Edge states attract more and more research interests owing to the novel topologically protected properties. In this work, we studied edge modes and traveling edge states via the linear Dirac equation with so-called edge-admissible masses. The unidirectional edge state provides a heuristic approach to more general traveling edge states through the localized behavior along slowly varying edges. We show the dominated asymptotic solutions of two typical edge states that follow circular and curved edges with small curvature by the analytic and quantitative arguments.

1. INTRODUCTION

The topological wave phenomena have sparked an explosion of the interface features between distinct topological insulators [3, 16, 17, 18, 27]. One striking character of the so-called edge states is the existence of chiral propagating waves which are immune to the local defects in the sense of waves retaining on the edge robustly. This immunity is a delicate property in applied perspectives and it can be contributed to interpreting many ubiquitous physical scenarios. These studies are not only investigated by the electronic waves in condensed matter physics but also rapidly extended to photonics, water waves and related subjects [15, 22, 24, 32, 34, 39, 41, 42].

In current work, we consider the dynamics of edge states described by the following two-component Dirac equation with a varying mass:

$$(1.1) \quad i\partial_t \begin{pmatrix} \alpha_1 \\ \alpha_2 \end{pmatrix} + \begin{pmatrix} m(\mathbf{x}) & \partial_- \\ \partial_+ & -m(\mathbf{x}) \end{pmatrix} \begin{pmatrix} \alpha_1 \\ \alpha_2 \end{pmatrix} = 0, \quad (t > 0, \mathbf{x} \in \mathbb{R}^2),$$

where $\alpha_j = \alpha_j(t, \mathbf{x})$, $j = 1, 2$ are complex-valued wave functions, $m(\mathbf{x}) \in C(\mathbb{R}^2, \mathbb{R})$ is the mass term, “ i ” is the imaginary unit, and

$$\partial_{\pm} = i\partial_{x_1} \pm \partial_{x_2}.$$

In homogeneous honeycomb latticed materials, Dirac points regularly appear at the spectrum band structure with the corresponding quasi-periodic eigenmodes and the wave packets around this degenerated point will be dominated by the massless Dirac equation [1, 2, 20, 21, 23, 30, 35, 36, 37]. However, this conical intersection will bifurcate if time-reversal symmetry is broken in the material and then a local band gap emerges in the essential spectrum which leads to the insulating bulk [20, 26, 27, 38]. The Dirac equation with a varying mass (1.1) arises from the effective envelopes of wave propagation in topological materials. Here, the mass $m(\mathbf{x})$ determines the

Date: March 1, 2022.

2020 Mathematics Subject Classification. 35B40, 35C07, 35Q41, 78M35.

Key words and phrases. massive Dirac equation, charity, edge states, asymptotic solution.

distinct topology such that two adherent materials are topological insulators in bulks and the current or electromagnetic wave is permitted to travel along the contact edge [13, 28, 37, 43]. The associated edge, null domain of $m(\mathbf{x})$, separates the two dimensional materials with different topology in each part. Moreover, this novel electric conductivity elucidates the charity and one unidirectional localized current flows along the edge only. Recently, the spectrum structure in honeycomb latticed medium also fascinates lots of attention from mathematical viewpoint. A variety of rigorous research has studied the existence of Dirac points and the local band gap brought after a time reversal symmetry breaking perturbation in domain wall and tight binding models [6, 19, 20, 29, 30, 44]. Meanwhile, one dimensional topologically protected edge state (or namely interface mode) always occur at the band gap when two adjacent medium state the distinct topological invariant corresponding to Zak phase and Chern number [4, 5, 9, 16, 18, 25, 30, 31]. Instead of dealing with the highly oscillated interface mode directly, a canonical way is to exploit the essentially homogenized envelope emerged by the time-harmonic massive Dirac equation which expresses the topological protected properties more clearly and intuitively. Studies about the existence of edge states or the derivation of governed envelopes—Dirac equations are carried out in many settings, such as microlocal analysis, transfer matrix method, Fredholm operator index, K-theory, and so on [7, 8, 9, 16, 31, 40].

In many physical applications, edge modes would also travel along various shapes of the interface where bulk defects happen [12, 14, 33]. These physical phenomena stimulate the interests of wave propagation along the nontrivial edges. Recently, a class of Dirac equations with a small semi-classical parameter described the wave packets which propagate along the curved edge for long times [10, 11]. However, these effective models depend on the small parameter in the semi-classical equation and the curvature of nearly straight edge provides the limited effect to the time validity. Unlike the previous studies, we will introduce an edge-admissible mass term and directly elucidate the classical dynamics of edge states when the interface curvature is very small. We seek the asymptotic wave propagation pinned on the curved edge from the idea of modes along the straight interface and we also exploit a delicate modulation so that the accuracy of energy estimate will be improved.

For the convenience of study, let $\beta_1 = \alpha_1 + i\alpha_2$ and $\beta_2 = \alpha_1 - i\alpha_2$. Then, the equation (1.1) will switch to the following canonical form,

$$(1.2) \quad i\partial_t \begin{pmatrix} \beta_1 \\ \beta_2 \end{pmatrix} + \begin{pmatrix} i\partial_{x_2} & m(\mathbf{x}) - \partial_{x_1} \\ m(\mathbf{x}) + \partial_{x_1} & -i\partial_{x_2} \end{pmatrix} \begin{pmatrix} \beta_1 \\ \beta_2 \end{pmatrix} = 0.$$

One can directly verify that the total energy $\mathcal{E}(t) = \int_{\mathbb{R}^2} |\beta_1(t, \mathbf{x})|^2 + |\beta_2(t, \mathbf{x})|^2 d\mathbf{x}$ is conserved since the Dirac operator behaves as a Hamiltonian. It also admits the global existence for the smooth solution under a well-posed initial condition.

The crucial result in our development is the asymptotics to edge states that is guided by the slowly varying edge perfectly. It can be carried out through the constructively asymptotic solution which is locally raised from the case of straight mass edge. We employ a well-prepared initial condition and then we show a more accurate validity of this setup via the analytic and quantitative studies. From this scenario, it enlightens that the edge states governed by the macroscopic massive Dirac equation are topologically protected. The main results of the present work are summarized here:

- For the basic straight line edge, we employ the plane wave separation to discuss the unidirectional traveling edge state that is pinned on the edge in Proposition 2.5 and Corollary 2.7;
- For the slowly varying edge, we establish two typical traveling edge states along the circular ring with large radius and generic curves with the small curvature in Theorem 3.2 and Theorem 3.3 respectively. We demonstrate the reliability of herein developed asymptotic solutions and the residual errors only depend on time linearly and curvature quadratically.

The rest of this article is organized as follows. We discuss the solution to the traveling edge state described by the unidirectional edge-admissible massive Dirac equation in Section 2. In Section 3, two typical models with general edge-admissible masses show that the asymptotic solutions are heuristically solved by regarding the partial edge as a local straight line along the tangent direction.

2. TRAVELING EDGE STATES WITH THE LINEAR MASS

In the physical setup, the “edge” (or interface) comes from the connected boundary between two topological materials, and can be described by a smooth function [16, 30]. For this sake, we define the edge-admissible mass term:

Definition 2.1. The mass term $m(\mathbf{x})$ is edge-admissible if $m(\mathbf{x})$ can be written as $m(\mathbf{x}) = \tilde{m}(u)$, $u = f(\mathbf{x})$ or equivalently $\tilde{m}(f(\mathbf{x}))$ satisfies the following conditions:

- (1) The level set $\Gamma = \{\mathbf{x} \in \mathbb{R}^2 : f(\mathbf{x}) = 0\} = \tilde{m}^{-1}(0)$ represents a smooth curve in (x_1, x_2) plane;
- (2) $\tilde{m}(\cdot) \in L^\infty(\mathbb{R})$ is a transition function and $\lim_{u \rightarrow \pm\infty} \tilde{m}(u) = \pm m_\infty$, $m_\infty > 0$, i.e., the mass term approximates to a constant rapidly when \mathbf{x} is away from the edge curve Γ .

Remark 2.2. In previous works, there was the concept of “domain wall” to describe the quality item with “edge” [19, 20, 30]. Here we mainly focus on the propagation of edge states along various edges. To describe the mathematical characteristics of complex edges more concisely, we introduce the definition of the “edge-admissible” term. It is consistent with the concept of domain walls, while the related edge features will be further described.

Now, we review two typical examples of transition functions in edge-admissible mass terms from the literature [19, 20, 30].

Example 2.3. $\tilde{m}(u) = \tanh(u)$.

Example 2.4.

$$\tilde{m}(u) = \begin{cases} -1, & \text{for } u < 0, \\ 0, & \text{for } u = 0, \\ 1, & \text{for } u > 0. \end{cases}$$

From now on, we will drop the tilde hat and study a specified edge-admissible mass term for simplicity, i.e., the mass term is denoted by $m(f(\mathbf{x}))$ with the edge $\Gamma = \{\mathbf{x} \in \mathbb{R}^2 : f(\mathbf{x}) = 0\}$.

Now, we reveal the edge states with a linear edge $\Gamma = \{\mathbf{x} \in \mathbb{R}^2 : x_2 = cx_1\}$ and the Dirac equation has an explicit traveling wave solution. To this end, we assume that $m(f(\mathbf{x})) = m(\hat{\mathbf{n}} \cdot \mathbf{x})$ where $\hat{\mathbf{n}} = \frac{1}{\sqrt{c^2+1}}(c, -1)^T$ is a unit normal vector to the

edge. Figure 1A shows a vertical straight edge and Figure 1B is a general linear case. We rewrite (1.2) in the linear edge form:

$$(2.1) \quad i\partial_t \begin{pmatrix} \beta_1 \\ \beta_2 \end{pmatrix} + \begin{pmatrix} i\partial_{x_2} & m(\hat{\mathbf{n}} \cdot \mathbf{x}) - \partial_{x_1} \\ m(\hat{\mathbf{n}} \cdot \mathbf{x}) + \partial_{x_1} & -i\partial_{x_2} \end{pmatrix} \begin{pmatrix} \beta_1 \\ \beta_2 \end{pmatrix} = 0.$$

Further, by introducing the azimuth $\theta \in (0, 2\pi)$ to x -axis and the tangent vector $\hat{\mathbf{t}}$ of the edge, we have

$$(2.2) \quad \hat{\mathbf{n}} = \begin{pmatrix} \cos \theta \\ \sin \theta \end{pmatrix}, \quad \hat{\mathbf{t}} = \begin{pmatrix} -\sin \theta \\ \cos \theta \end{pmatrix}.$$

Recall that the mass term is edge-admissible by Definition 2.1, $m(u)$ rapidly approaches to $\pm m_\infty$ as $u = \hat{\mathbf{n}} \cdot \mathbf{x} \rightarrow \pm\infty$.

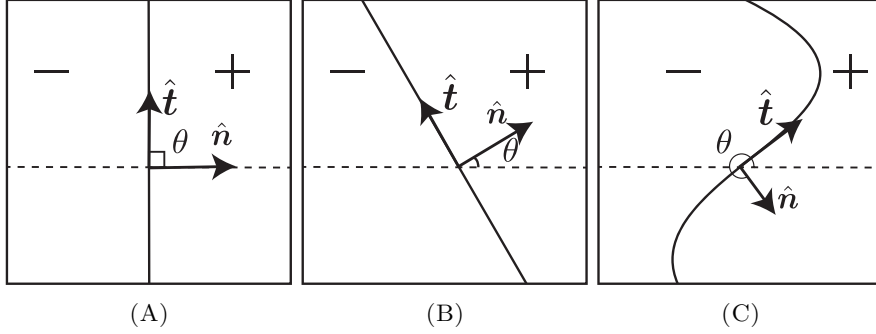


FIGURE 1. Left panel (a): the vertical straight line edge. Middle panel (b): the general case of straight line edge. Right panel (c): the general case of curved edge.

We would reveal the edge states with linear masses and the Dirac equation (2.1) has plane wave solutions. The result is summarized below.

Proposition 2.5. For any unit normal vector $\hat{\mathbf{n}} \in \mathbb{R}^2$ and energy parameter $\lambda \in \mathbb{R}$, the Dirac equation (2.1) has a plane wave solution

$$(2.3) \quad \begin{pmatrix} \beta_1 \\ \beta_2 \end{pmatrix} = \chi(\hat{\mathbf{n}} \cdot \mathbf{x}) e^{i\lambda(\hat{\mathbf{t}} \cdot \mathbf{x} - t)} \begin{pmatrix} \cos \frac{\theta}{2} \\ i \sin \frac{\theta}{2} \end{pmatrix},$$

where $\chi(u) = C e^{-\int_0^u m(s) ds}$ is a localized real-valued function with $C > 0$ being the normalization constant. Moreover, $\begin{pmatrix} \chi(u) \\ 0 \end{pmatrix}$ is an eigenfunction corresponding to the eigenvalue $-\lambda$ of the following one-dimensional (1D) Dirac operator

$$(2.4) \quad \mathcal{D}_\lambda = \begin{pmatrix} -\lambda & m(u) - \partial_u \\ m(u) + \partial_u & \lambda \end{pmatrix}.$$

Proof. We firstly perform the coordinate transformation,

$$(2.5) \quad u = \hat{\mathbf{n}} \cdot \mathbf{x}, \quad v = \hat{\mathbf{t}} \cdot \mathbf{x},$$

or equivalently by (2.2)

$$\begin{pmatrix} u \\ v \end{pmatrix} = \begin{pmatrix} \cos \theta & \sin \theta \\ -\sin \theta & \cos \theta \end{pmatrix} \begin{pmatrix} x_1 \\ x_2 \end{pmatrix}.$$

Let $\tilde{\beta}_j(t, u, v) = \beta_j(t, \mathbf{x}(u, v))$, $j = 1, 2$. The Dirac equation (2.1) changes into

$$(2.6) \quad i\partial_t \begin{pmatrix} \tilde{\beta}_1 \\ \tilde{\beta}_2 \end{pmatrix} + \tilde{\mathcal{D}} \begin{pmatrix} \tilde{\beta}_1 \\ \tilde{\beta}_2 \end{pmatrix} = 0.$$

Here, the Dirac operator $\tilde{\mathcal{D}}$ under the new coordinate is in the form of

$$\tilde{\mathcal{D}} = \begin{pmatrix} i(\sin \theta \partial_u + \cos \theta \partial_v) & m(u) - (\cos \theta \partial_u - \sin \theta \partial_v) \\ m(u) + (\cos \theta \partial_u - \sin \theta \partial_v) & -i(\sin \theta \partial_u + \cos \theta \partial_v) \end{pmatrix}.$$

However, $\tilde{\mathcal{D}}$ looks obscure by messing with θ . To make it clear, we introduce a rotation transformation such that $\phi_j = \phi_j(t, u, v)$, $j = 1, 2$ satisfy

$$(2.7) \quad \begin{pmatrix} \phi_1 \\ \phi_2 \end{pmatrix} = S \begin{pmatrix} \tilde{\beta}_1 \\ \tilde{\beta}_2 \end{pmatrix} \quad \text{and} \quad S = \begin{pmatrix} \cos \frac{\theta}{2} & -i \sin \frac{\theta}{2} \\ -i \sin \frac{\theta}{2} & \cos \frac{\theta}{2} \end{pmatrix}.$$

Here $S^*S = I$ and the asterisk $*$ indicates the conjugate transpose. Then, a direct calculation yields (2.6) into

$$(2.8) \quad i\partial_t \begin{pmatrix} \phi_1 \\ \phi_2 \end{pmatrix} + \begin{pmatrix} i\partial_v & m(u) - \partial_u \\ m(u) + \partial_u & -i\partial_v \end{pmatrix} \begin{pmatrix} \phi_1 \\ \phi_2 \end{pmatrix} = 0,$$

which is parallel to the standard form (2.1) when $\theta = 0$ shown in Figure 1A.

Substituting $\phi_j(t, u, v) = \tilde{\phi}_j(u)e^{i\lambda v + i\omega t}$, $j = 1, 2$ into the above equation (2.8) develops an eigenvalue problem to the 1D Dirac operator,

$$(2.9) \quad \mathcal{D}_\lambda \tilde{\phi} = \omega \tilde{\phi}, \quad \tilde{\phi} = \begin{pmatrix} \tilde{\phi}_1 \\ \tilde{\phi}_2 \end{pmatrix},$$

where the Dirac operator \mathcal{D}_λ is defined in Proposition 2.5. Namely, we have

$$\partial_u \tilde{\phi} = m(u) \begin{pmatrix} -1 & 0 \\ 0 & 1 \end{pmatrix} \tilde{\phi} + \begin{pmatrix} 0 & -(\lambda - \omega) \\ -(\lambda + \omega) & 0 \end{pmatrix} \tilde{\phi}.$$

From the right-hand side, the eigenvalues of the second matrix are $\pm\sqrt{\lambda^2 - \omega^2}$ and the corresponding eigenvectors are

$$\mathbf{v}_1 = \begin{pmatrix} \lambda - \omega + \sqrt{\lambda^2 - \omega^2} \\ -\sqrt{\lambda^2 - \omega^2} - (\lambda + \omega) \end{pmatrix}, \quad \mathbf{v}_2 = \begin{pmatrix} \lambda - \omega + \sqrt{\lambda^2 - \omega^2} \\ \sqrt{\lambda^2 - \omega^2} + \lambda + \omega \end{pmatrix}.$$

Therefore, $\tilde{\phi}$ can be written as the composition of $\chi_1(u)\mathbf{v}_1 + \chi_2(u)\mathbf{v}_2$. However, the localized solution only exists when $\omega = -\lambda$ and

$$(2.10) \quad \tilde{\phi} = \begin{pmatrix} \chi(u) \\ 0 \end{pmatrix}, \quad \chi(u) = Ce^{-\int_0^u m(\tau) d\tau}.$$

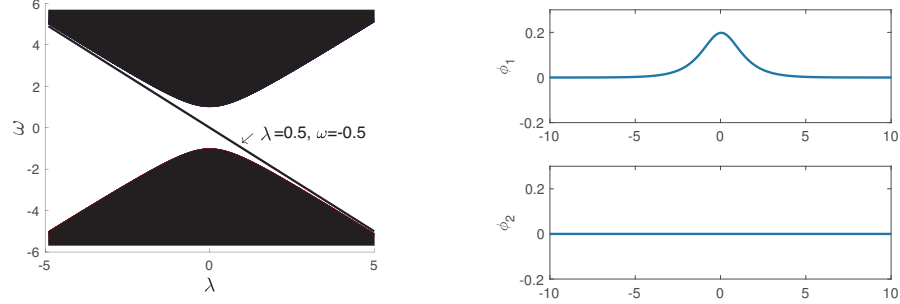
Here C is the normalized coefficient. We refer to [30, 43] for details.

Remark 2.6. Specifically, if $m(\mathbf{x}) = \tanh x_1$, the dispersion relationship and the localized eigenfunctions are simulated in Figure 2.

We immediately derive the plane wave solution of (2.8) as

$$(2.11) \quad \begin{pmatrix} \tilde{\phi}_1 \\ \tilde{\phi}_2 \end{pmatrix} = \chi(u)e^{i\lambda(v-t)} \begin{pmatrix} 1 \\ 0 \end{pmatrix}.$$

Applying the inverse transform of (2.7) to (2.11), we eventually obtain the plane wave solution (2.3). This completes the proof. \square



(A) Eigenvalue of the Dirac operator \mathcal{D}_λ , where the straight line $\omega = -\lambda$ results in the localized mode and the shadow area contributes to the oscillation modes.

(B) Eigenfunction at $\lambda = 0.5$

FIGURE 2. The Edge Eigen for $m(\mathbf{x}) = \tanh x_1$

The dispersion curve $\omega(\lambda)$ corresponding to the localized eigenfunction is a straight line with the slope -1 , which means the modes of the form (2.3) with different wavenumber λ has the same group velocity $v_{\text{group}} = -\frac{\partial\omega(\lambda)}{\partial\lambda} = 1$ (note that the energy parameter ω selected here differs from the settings in physics by a negative sign). A similar discussion as the above plane wave result carries out the localized solution in next corollary.

Corollary 2.7. Let the continuous function $g(\cdot) \in L^2(\mathbb{R})$. If the initial input to the edge of problem (2.1) is in the following localized form

$$\begin{pmatrix} \beta_1(0, \mathbf{x}) \\ \beta_2(0, \mathbf{x}) \end{pmatrix} = \chi(\hat{\mathbf{n}} \cdot \mathbf{x}) g(\hat{\mathbf{t}} \cdot \mathbf{x}) \begin{pmatrix} \cos \frac{\theta}{2} \\ i \sin \frac{\theta}{2} \end{pmatrix}.$$

Then, the localized traveling wave solution admits

$$(2.12) \quad \begin{pmatrix} \beta_1(t, \mathbf{x}) \\ \beta_2(t, \mathbf{x}) \end{pmatrix} = \chi(\hat{\mathbf{n}} \cdot \mathbf{x}) g(\hat{\mathbf{t}} \cdot \mathbf{x} - t) \begin{pmatrix} \cos \frac{\theta}{2} \\ i \sin \frac{\theta}{2} \end{pmatrix}.$$

This is a one way traveling wave along the edge with the velocity $v = -\frac{\partial\omega}{\partial\lambda} = 1$. Till now, we have built the exact traveling localized waves along a straight edge through the separation of variables. However, it is quite involved to derive the traveling waves with a general mass. If $m(f(\mathbf{x}))$ is edge-admissible with the edge curve Γ slowly varying, a robust edge state can be asymptotically approached by treating the edge curve as a local straight line towards its tangential direction.

3. TWO TYPICAL ASYMPTOTIC EDGE STATES

Among the general edge-admissible mass terms, we asymptotically propose two typical edge states where the edges can be locally treated as straight lines. Here, we exploit the explicit asymptotic behaviors that cling to the edges locally other than solving the wave guidance derived from ODE [10, 11]. In the next two subsections, one edge is a circular ring with the sufficiently large radius, and another is a slowly varying curve which is generated by adding a small perturbation to the straight line on the normal direction.

3.1. Asymptotics to the edge states along a circular ring. Suppose that the mass term remains invariantly along the angular direction in polar coordinates, i.e., the edge curve is a circular ring. Therefore, the mass term can be described by

$$(3.1) \quad m(f(\mathbf{x})) = m(\sqrt{x_1^2 + x_2^2} - R),$$

where $R \in (0, +\infty)$ is a fixed radius of the circle. Let the reference system alter into the polarization coordinates $x_1 = r \cos \theta$, $x_2 = r \sin \theta$ with $r \in [0, +\infty)$, $\theta \in [0, 2\pi)$. Without loss of generality, we assume that $\exists 0 < r_0 < 1$, $|m(u)| > \frac{m_\infty}{2}$ provided $|u| > r_0$.

In such a case, the Dirac equation (2.1) under the polarization coordinates admits the following form,

$$(3.2) \quad i\partial_t \beta + \tilde{D}\beta = \mathbf{0},$$

where $\beta = \begin{pmatrix} \beta_1 \\ \beta_2 \end{pmatrix}$, $\beta_j = \beta_j(t, r, \theta)$, $j = 1, 2$, and the new Dirac operator is

$$(3.3) \quad \tilde{D} = \begin{pmatrix} i \sin \theta \partial_r + \frac{i}{r} \cos \theta \partial_\theta & m(r - R) - \cos \theta \partial_r + \frac{1}{r} \sin \theta \partial_\theta \\ m(r - R) + \cos \theta \partial_r - \frac{1}{r} \sin \theta \partial_\theta & -i \sin \theta \partial_r - \frac{i}{r} \cos \theta \partial_\theta \end{pmatrix}.$$

Moreover, $e^{i\tilde{D}t}$ also represents a Dirac group and is unitary in $L^2(\mathbb{R}^2)$ for all $t \in \mathbb{R}^+$.

Observe that the traveling wave solution to the Dirac equation (2.1) is of the form (2.12). With a circular ring edge, it is not surprising that we set up the following traveling wave solution ansatz by treating the circle as a straight line locally.

Proposition 3.1. Let $R > 0$ be a sufficiently large radius. Given the initial condition of Dirac equation (3.2),

$$(3.4) \quad \begin{pmatrix} \beta_1(0, r, \theta) \\ \beta_2(0, r, \theta) \end{pmatrix} = \phi(r)g(\theta) \begin{pmatrix} \cos \frac{\theta}{2} \\ i \sin \frac{\theta}{2} \end{pmatrix},$$

where $g \in C^1([0, 2\pi])$ with $g(2\pi) = g(0)$ and $\phi(r) \in C^1([0, +\infty))$ is a localized function around $r = R$. Then, there exists an asymptotic solution to the Dirac equation (3.2),

$$(3.5) \quad \begin{pmatrix} \beta_1(t, r, \theta) \\ \beta_2(t, r, \theta) \end{pmatrix} \sim \phi(r)g\left(\theta - \frac{t}{R}\right) \begin{pmatrix} \cos \frac{\theta}{2} \\ i \sin \frac{\theta}{2} \end{pmatrix}.$$

We need to derive the validity of the above approximation. Plugging the right hand side of (3.5) into the equation (3.2) deduces the residual terms as

$$(3.6) \quad RHS = \begin{pmatrix} i(\phi' + m\phi + \frac{1}{2r}\phi)g \sin \frac{\theta}{2} + i(\frac{1}{r} - \frac{1}{R})\phi g' \cos \frac{\theta}{2} \\ (\phi' + m\phi + \frac{1}{2r}\phi)g \cos \frac{\theta}{2} - (\frac{1}{r} - \frac{1}{R})\phi g' \sin \frac{\theta}{2} \end{pmatrix}.$$

Some extra constraints on $\phi(r)$ are needed as $r \rightarrow 0^+$, otherwise RHS may lead to singularities at the original.

Now, we give a rigorous clarification for the asymptotic solution to the edge states pinned on the circular ring.

Theorem 3.2. *The Dirac equation (3.2) is spacially defined in the polar coordinates with the circular edge-admissible mass (3.1), where the radius $R > 3r_0$. Moreover, $\phi(r) \in C^1([0, +\infty))$ and satisfies:*

$$(1) \text{ if } r \in [0, \frac{R}{3}], \phi(r) = 0;$$

- (2) if $r \in (\frac{R}{3}, \frac{R}{2})$, $|\phi'(r)| < \frac{12}{R}\phi(\frac{R}{2})$;
(3) if $r \in [\frac{R}{2}, +\infty)$, $\phi(r) = \frac{1}{\sqrt{R}}\chi(r-R)e^{-\frac{r}{2R}}$, where $\chi(\cdot)$ is defined in Proposition 2.5 and $\frac{1}{\sqrt{R}}$ is the normalized parameter in $L^2(\mathbb{R}^2)$.

Suppose that the initial condition is of the form (3.4) stated in Proposition 3.1. Then, for any $t > 0$, there is a constant $C > 0$ independent of t, R such that

$$\left\| \begin{pmatrix} \beta_1(t, r, \theta) \\ \beta_2(t, r, \theta) \end{pmatrix} - \phi(r)g\left(\theta - \frac{t}{R}\right) \begin{pmatrix} \cos \frac{\theta}{2} \\ i \sin \frac{\theta}{2} \end{pmatrix} \right\|_{L^2(\mathbb{R}^2)} \leq Ct \frac{1}{R^2}.$$

Proof. Let $\boldsymbol{\eta} = \boldsymbol{\eta}(t, r, \theta)$ indicate the error of the asymptotic solution (3.5), i.e.,

$$\boldsymbol{\eta} = \begin{pmatrix} \beta_1(t, r, \theta) \\ \beta_2(t, r, \theta) \end{pmatrix} - \phi(r)g\left(\theta - \frac{t}{R}\right) \begin{pmatrix} \cos \frac{\theta}{2} \\ i \sin \frac{\theta}{2} \end{pmatrix}.$$

Owing to RHS given in (3.6), the error $\boldsymbol{\eta}$ evolves like:

$$i\partial_t \boldsymbol{\eta} + \tilde{\mathcal{D}} \boldsymbol{\eta} = -RHS.$$

Then, it follows from the Duhamel's principle that

$$\boldsymbol{\eta} = i \int_0^t e^{i\tilde{\mathcal{D}}(t-s)} RHS \, ds, \quad \forall t > 0.$$

According to the fact that $e^{i\tilde{\mathcal{D}}t}$ is unitary in $L^2(\mathbb{R}^2)$, we can directly obtain

$$(3.7) \quad \|\boldsymbol{\eta}\|_{L^2(\mathbb{R}^2)} \leq \int_0^t \|RHS\|_{L^2(\mathbb{R}^2)} \, ds.$$

As it has been stated before, if $0 \leq r \leq \frac{R}{3}$, $\phi(r) \equiv 0$. When $r \in (\frac{R}{3}, \frac{R}{2})$, for any $n \geq 0$, it implies

$$|\phi' + m\phi + \frac{1}{2r}\phi| \leq C \frac{1}{R^n}, \quad |(\frac{1}{r} - \frac{1}{R})\phi| \leq C \frac{1}{R^n}.$$

Here the constants C are independent of R .

If $r \geq \frac{R}{2}$, we have

$$\phi' + m\phi = -\frac{1}{2R}\phi.$$

Then, for $r \in [\frac{R}{2}, R - r_0] \cup [R + r_0, +\infty)$, it follows that

$$|(\frac{1}{r} - \frac{1}{R})\phi(r)| \leq C \frac{|R - r|}{rR^{\frac{3}{2}}} e^{-\frac{m_\infty}{2}|R - r|}.$$

Noting the boundedness of $\chi(\cdot)$, we claim the result below as $r \in (R - r_0, R + r_0)$,

$$|(\frac{1}{r} - \frac{1}{R})\phi(r)| \leq C \frac{1}{R^{\frac{3}{2}}},$$

which also implies why we brought the modulated factor $e^{-\frac{r}{2R}}$ into $\phi_R(r)$.

Consequently, for any $t > 0$, it turns out that

$$\begin{aligned} \|RHS\|_{L^2(\mathbb{R}^2)}^2 &\leq C \int_0^{2\pi} \int_0^{+\infty} \left[|\phi' + m\phi + \frac{1}{2r}\phi|^2 + |(\frac{1}{r} - \frac{1}{R})\phi g'|^2 \right] r dr d\theta \\ &\leq C \int_{\frac{R}{3}}^{\frac{R}{2}} \left[|\phi' + m\phi + \frac{1}{2r}\phi|^2 + |(\frac{1}{r} - \frac{1}{R})\phi|^2 \right] r dr d\theta \end{aligned}$$

$$\begin{aligned}
& + C \int_{\frac{R}{2}}^{+\infty} \left| \left(\frac{1}{r} - \frac{1}{R} \right) \phi \right|^2 r dr d\theta \\
& \leq C \frac{1}{R^{2n}} + C \frac{1}{R^4} \\
& \leq C \frac{1}{R^4}.
\end{aligned}$$

Here we choose $n \geq 2$ to ensure the estimate consistently.

According to the formula in (3.7), for any $t > 0$, we have

$$\|\boldsymbol{\eta}\|_{L^2(\mathbb{R}^2)} \leq Ct \frac{1}{R^2}.$$

This completes the proof. \square

To support our analysis, we also numerically compute the traveling waves to the Dirac equation (3.2) with the initial condition (3.4). With different radius, we compute the error “*Err*” of asymptotic solution (3.5) at the same time and it indicates that *Err* goes like $\mathcal{O}(\frac{1}{R^2})$ in $L^2(\mathbb{R}^2)$ as shown in Figure 3. In Figure 4, it carries out the numerical simulation patterns for two circular edges with different radii $R = 20, 40$ respectively. The waves travel around circles with negligible energy leaking into the bulk as $R > 0$ large enough. The traveling directions obey the chiral property, which leave the positive mass on the right.

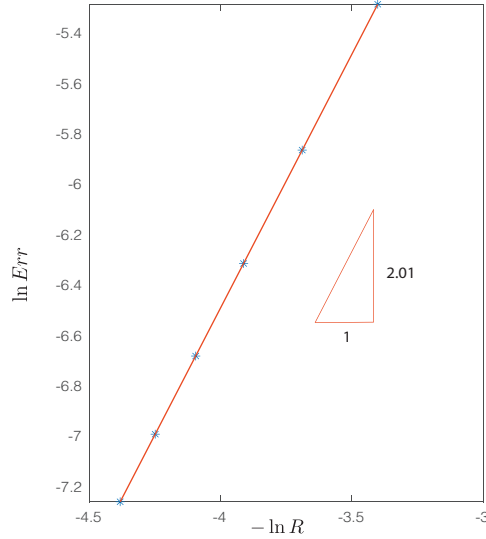


FIGURE 3. The numerical results of the L^2 error for the circle-curved edge state show the decay rate in the order of $\mathcal{O}(\frac{1}{R^2})$ at $T = 5$. The fit function admits $\ln Err = -2.01 \ln R + 1.56$.

3.2. Asymptotics to the smooth-curved edge state. In this section, we consider a family of more universal edge states which highly propagate along the smooth edge-admissible curves. Observe that the straight line edge state with the rotation angle θ admits the propagating form of (2.12). In Figure 1C, the smooth edge curve can be locally treated as the tangent line. It sheds some light on that the

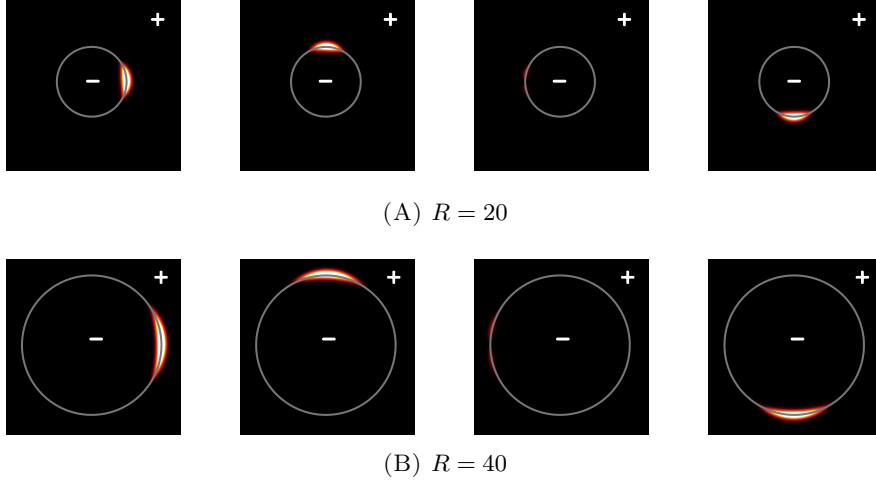


FIGURE 4. Traveling waves of $|\beta_1|^2$ with two different circular radius at four successive time: $T = 0, \frac{\pi R}{2}, \pi R, \frac{3\pi R}{2}$. Top four subfigures (A): $R = 20$. Bottom four subfigures (B): $R = 40$.

curved edge states may comply with the localized solution traveling along the tangent direction on the curve. Hence, we study the asymptotic traveling waves when the straight edge-admissible curve is slowly disturbed.

Assume that the edge curve is a small perturbation to the vertical line, i.e.,

$$(3.8) \quad \Gamma = \{\mathbf{x} \in \mathbb{R}^2 : x_1 + h(\varepsilon x_2) = 0\}.$$

Here $0 < \varepsilon \ll 1$ and $h(\varepsilon x_2)$ indicates the small perturbation to the straight line. Other more general edge curves can be treated similarly by coordinate rotation. After that, the Dirac operator with the curved edge-admissible mass $m(x_1 + h(\varepsilon x_2))$ is in the form of

$$\mathcal{D}^\varepsilon = \begin{pmatrix} i\partial_{x_2} & m(x_1 + h(\varepsilon x_2)) - \partial_{x_1} \\ m(x_1 + h(\varepsilon x_2)) + \partial_{x_1} & -i\partial_{x_2} \end{pmatrix}.$$

Therefore, the Dirac equation (2.1) alters into

$$(3.9) \quad i\partial_t \begin{pmatrix} \beta_1 \\ \beta_2 \end{pmatrix} + \mathcal{D}^\varepsilon \begin{pmatrix} \beta_1 \\ \beta_2 \end{pmatrix} = 0.$$

Under this setup, we move forward to establish the smooth edge state in an asymptotic way. Recalling the edge curve equation in (3.8) generates the unit normal and tangent vectors at each point on the curve:

$$\begin{aligned} \hat{\mathbf{n}} &= \frac{1}{\sqrt{1 + \varepsilon^2 h'^2(\varepsilon x_2)}} \begin{pmatrix} 1 \\ \varepsilon h'(\varepsilon x_2) \end{pmatrix} = \begin{pmatrix} 1 \\ \varepsilon h'(\varepsilon x_2) \end{pmatrix} + \mathcal{O}(\varepsilon^2), \\ \hat{\mathbf{t}} &= \frac{1}{\sqrt{1 + \varepsilon^2 h'^2(\varepsilon x_2)}} \begin{pmatrix} -\varepsilon h'(\varepsilon x_2) \\ 1 \end{pmatrix} = \begin{pmatrix} -\varepsilon h'(\varepsilon x_2) \\ 1 \end{pmatrix} + \mathcal{O}(\varepsilon^2). \end{aligned}$$

With the help of the straight line edge state (2.12), it is not surprising to develop an analogous result traveling along the slowly varying edge. From the curve function

(3.8) and the above tangent vector $\hat{\mathbf{t}}$, it yields the asymptotic solution as follows:

$$(3.10) \quad \begin{pmatrix} \beta_1 \\ \beta_2 \end{pmatrix}_\varepsilon = \chi(x_1 + h(\varepsilon x_2))g(-\varepsilon h'(\varepsilon x_2)(x_1 + h(\varepsilon x_2)) + x_2 - t) \begin{pmatrix} 1 \\ \frac{i}{2}\varepsilon h'(\varepsilon x_2) \end{pmatrix}.$$

The validity of this construction can be demonstrated up to $\mathcal{O}(\varepsilon^2)$ below.

Theorem 3.3. *Let $0 < \varepsilon \ll 1$, $\chi(\cdot)$ be denoted as (2.10) and $g(\cdot) \in \mathcal{S}(\mathbb{R})$. The mass term $m(\cdot)$ with the edge curve Γ defined by (3.8) is edge-admissible. The edge perturbation $h(\cdot) \in C^2(\mathbb{R})$ and $h'(\cdot)$, $h''(\cdot)$ are both bounded on \mathbb{R} . Suppose that the initial condition is perfectly matched, i.e., $\begin{pmatrix} \beta_1 \\ \beta_2 \end{pmatrix}(0, \mathbf{x}) = \begin{pmatrix} \beta_1 \\ \beta_2 \end{pmatrix}_\varepsilon(0, \mathbf{x})$. Then for any $t > 0$,*

$$\left\| \begin{pmatrix} \beta_1 \\ \beta_2 \end{pmatrix}(t, \mathbf{x}) - \begin{pmatrix} \beta_1 \\ \beta_2 \end{pmatrix}_\varepsilon(t, \mathbf{x}) \right\|_{L^2(\mathbb{R}^2)} < Ct\varepsilon^2.$$

Here C is a generic constant independent of t and ε .

Proof. Let the error $\boldsymbol{\eta}(t, \mathbf{x}) = \begin{pmatrix} \beta_1 \\ \beta_2 \end{pmatrix}(t, \mathbf{x}) - \begin{pmatrix} \beta_1 \\ \beta_2 \end{pmatrix}_\varepsilon(t, \mathbf{x})$. Substituting the above formal solution (3.10) into (3.9), the evolution of $\boldsymbol{\eta}(t, \mathbf{x})$ arrives at

$$i\partial_t \boldsymbol{\eta} + \mathcal{D}^\varepsilon \boldsymbol{\eta} = -\frac{1}{2}\varepsilon^2 \begin{pmatrix} -i2(x_1 + h)\chi g' h'' - i\chi g' h'^2 \\ \chi g h'' + \chi' g h'^2 - \varepsilon(x_1 + h)\chi g' h' h'' - \varepsilon \chi g' h'^3 \end{pmatrix}.$$

By employing the same procedure in previous circular edge arguments, it suffices to estimate the above residuals.

For convenience, we employ the coordinate transformation by letting $y_1 = x_1 + h(\varepsilon x_2)$, $y_2 = x_2$, and then the Jacobi determinant is identically equal to 1. Assume that $|h'(\cdot)| \leq C_1$ uniformly on \mathbb{R} . For any $t > 0$, we firstly build the following estimate:

$$\begin{aligned} & \int_{\mathbb{R}^2} \left| \chi(y_1)g(-\varepsilon y_1 h'(\varepsilon y_2) + y_2 - t) \right|^2 d\mathbf{y} \\ &= \int_{\mathbb{R}} \left(\int_{|y_2 - t| > 2C_1 \varepsilon |y_1|} + \int_{|y_2 - t| \leq 2C_1 \varepsilon |y_1|} \right) \left| \chi(y_1)g(-\varepsilon y_1 h'(\varepsilon y_2) + y_2 - t) \right|^2 dy_2 dy_1 \\ &\leq C \int_{\mathbb{R}} \int_{|y_2 - t| > 2C_1 \varepsilon |y_1|} \chi^2(y_1) \frac{1}{1 + \left| \frac{y_2 - t}{2} \right|^2} dy_2 dy_1 + C \int_{\mathbb{R}} \int_{|y_2 - t| \leq 2C_1 \varepsilon |y_1|} \chi^2(y_1) dy_2 dy_1 \\ &\leq C \int_{\mathbb{R}^2} \chi^2(y_1) \frac{1}{1 + \left| \frac{y_2 - t}{2} \right|^2} d\mathbf{y} + C \int_{\mathbb{R}} \varepsilon |y_1| \chi^2(y_1) dy_1 \\ &\leq C < +\infty. \end{aligned}$$

Here we use the rapidly decreasing property of $\chi(\cdot)$ and $g(\cdot)$. Hence, for any $t > 0$, $\begin{pmatrix} \beta_1 \\ \beta_2 \end{pmatrix}_\varepsilon(t, \mathbf{x}) \in L^2(\mathbb{R}^2)^2$ and a similar strategy gives estimates to the residual,

$$\begin{aligned} & \left\| \begin{pmatrix} -i2(x_1 + h)\chi g' h'' - i\chi g' h'^2 \\ \chi g h'' + \chi' g h'^2 - \varepsilon(x_1 + h)\chi g' h' h'' - \varepsilon \chi g' h'^3 \end{pmatrix} \right\|_{L^2(\mathbb{R}^2)} \\ &= \left\| \begin{pmatrix} -i2y_1 \chi g' h'' - i\chi g' h'^2 \\ \chi g h'' + \chi' g h'^2 - \varepsilon y_1 \chi g' h' h'' - \varepsilon \chi g' h'^3 \end{pmatrix} \right\|_{L^2(\mathbb{R}^2)} < +\infty. \end{aligned}$$

Thanks to the fact that $e^{i\mathcal{D}^\varepsilon t}$ is unitary in $L^2(\mathbb{R}^2)$, we can directly move forward to conclude that

$$\|\boldsymbol{\eta}(t, \mathbf{x})\|_{L^2(\mathbb{R}^2)} < Ct\varepsilon^2, \quad \forall t > 0,$$

where C is a generic constant.

□

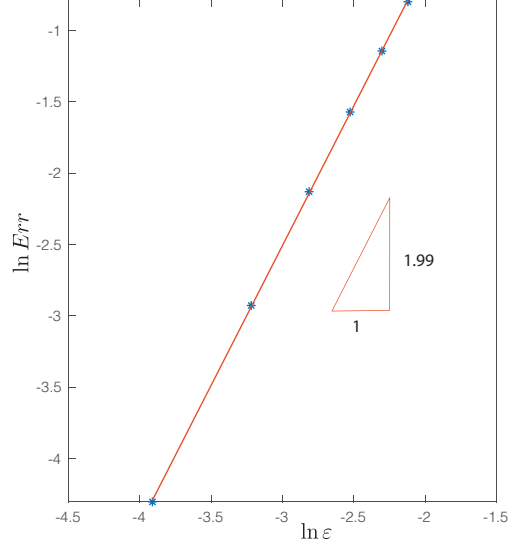


FIGURE 5. The numerical results of the L^2 error for the smooth-curved edge state show the decay rate in the order of $\mathcal{O}(\varepsilon^2)$ at $T = 5$. The fit equation is $\ln Err = 1.99 \ln \varepsilon + 2.78$.

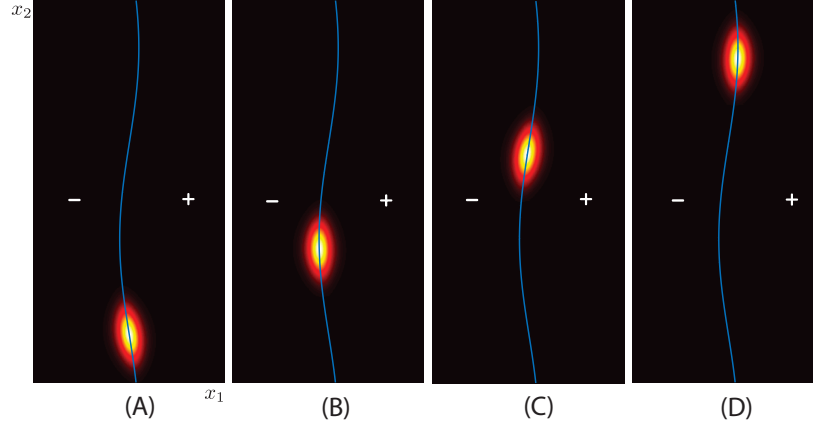


FIGURE 6. The energy of traveling waves along a smooth-curved edge $x_1 = -\sin(0.2x_2)$ in the domain $[-10, 10] \times [-10\pi, 10\pi]$ at four successive time: $T = 0, 10, 15, 20$.

From the above theorem, we establish the asymptotic traveling edge state along the smooth-curved admissible edge which arises from a perturbation to a straight line. Similarly, edge states traveling along arbitrary slowly varying curves also could be extended by the same coordinate transformation shown in the argument of Proposition 2.5.

4. CONCLUSION

By defining the edge-admissible mass terms, we studied the topologically protected edge states via the Dirac equation with such generic masses. In this work, the traveling edge state tracking a straight line stays localized and keeps its shape along with the movement, which also is related to the chiral property. This peculiar feature of the explicit solution gives an insight into investigating the Dirac equation with more general smooth edges. The edge state moving along a varying edge will be very robust provided that the edge curvature is sufficiently small and there is negligible energy leaking into the bulk. To explain this subtle phenomenon, we introduced two typical edges which one is a large circle and another is obtained by a small perturbation to a straight line. Our rigorous study and numerical simulation demonstrated the edge states remain almost unchanged and highly concentrated on the slowly varying edge curves over a long time.

5. ACKNOWLEDGEMENTS

This work was partially supported by the National Natural Science Foundation of China (grant #11871299). P. Xie would acknowledge the support from Professor Hai Zhang and Department of Mathematics at HKUST.

REFERENCES

- [1] M. J. Ablowitz, S. D. Nixon, and Y. Zhu. Conical diffraction in honeycomb lattices. *Physical Review A*, 79(5):053830, 2009.
- [2] M. J. Ablowitz and Y. Zhu. Nonlinear waves in shallow honeycomb lattices. *SIAM Journal on Applied Mathematics*, 72(1):240–260, 2012.
- [3] Mark J Ablowitz, Christopher W Curtis, and Yi Zhu. Localized nonlinear edge states in honeycomb lattices. *Physical Review A*, 88(1):013850, 2013.
- [4] H. Ammari, B. Davies, and E. O. Hiltunen. Robust edge modes in dislocated systems of subwavelength resonators. *arXiv preprint arXiv:2001.10455*, 2020.
- [5] H. Ammari, B. Davies, E. O. Hiltunen, and S. Yu. Topologically protected edge modes in one-dimensional chains of subwavelength resonators. *Journal de Mathématiques Pures et Appliquées*, 144:17–49, 2020.
- [6] H. Ammari, B. Fitzpatrick, E. O. Hiltunen, H. Lee, and S. Yu. Honeycomb-Lattice Minnaert Bubbles. *SIAM Journal on Mathematical Analysis*, 52(6):5441–5466, 2020.
- [7] G. Bal. Continuous bulk and interface description of topological insulators. *Journal of Mathematical Physics*, 60(8):081506, 2019.
- [8] G. Bal. Topological invariants for interface modes. *arXiv preprint arXiv:1906.08345*, 2019.
- [9] G. Bal. Topological protection of perturbed edge states. *Communications in Mathematical Sciences*, 17(1):193–225, 2019.
- [10] G. Bal, S. Becker, and A. Drouot. Magnetic slowdown of topological edge states. *arXiv preprint arXiv:2201.07133*, 2022.
- [11] G. Bal, S. Becker, A. Drouot, C. F. Kammerer, J. Lu, and A. Watson. Edge state dynamics along curved interfaces. *arXiv preprint arXiv:2106.00729*, 2021.
- [12] M. A. Bandres, M. C. Rechtsman, and M. Segev. Topological photonic quasicrystals: Fractal topological spectrum and protected transport. *Physical Review X*, 6(1):011016, 2016.
- [13] B. A. Bernevig. *Topological insulators and topological superconductors*. Princeton university press, 2013.
- [14] X. Cheng, C. Jouvaud, X. Ni, S. H. Mousavi, A. Z. Genack, and A. B. Khanikaev. Robust reconfigurable electromagnetic pathways within a photonic topological insulator. *Nature materials*, 15(5):542–548, 2016.
- [15] P. Delplace, J. B. Marston, and A. Venaille. Topological origin of equatorial waves. *Science*, 358(6366):1075–1077, 2017.
- [16] A. Drouot and M. I. Weinstein. Edge states and the valley Hall effect. *Adv. Math.*, 368:107142, 2020.

- [17] C. L. Fefferman, J. P. Lee-Thorp, and M. I. Weinstein. Bifurcations of edge states—topologically protected and non-protected—in continuous 2D honeycomb structures. *2D Materials*, 3(1):014008, 2016.
- [18] C. L. Fefferman, J. P. Lee-Thorp, and M. I. Weinstein. Edge states in honeycomb structures. *Annals of PDE*, 2(2):12, 2016.
- [19] C. L. Fefferman, J. P. Lee-Thorp, and M. I. Weinstein. *Topologically protected states in one-dimensional systems*, volume 247. Mem. Amer. Math. Soc., 2017.
- [20] C. L. Fefferman and M. I. Weinstein. Honeycomb lattice potentials and Dirac points. *J. Amer. Math. Soc.*, 25(4):1169–1220, 2012.
- [21] C. L. Fefferman and M. I. Weinstein. Wave packets in honeycomb structures and two-dimensional Dirac equations. *Comm. Math. Phys.*, 326(1):251–286, 2014.
- [22] R. Fleury, A. B. Khanikaev, and A. Alu. Floquet topological insulators for sound. *Nature communications*, 7(1):1–11, 2016.
- [23] A. K. Geim and K. S. Novoselov. The rise of graphene. *Nature Materials*, 6(3):183–91, 2007.
- [24] G. M. Graf, H. Jud, and C. Tauber. Topology in shallow-water waves: a violation of bulk-edge correspondence. *Communications in Mathematical Physics*, 383(2):731–761, 2021.
- [25] H. Guo, X. Yang, and Y. Zhu. Bloch theory-based gradient recovery method for computing topological edge modes in photonic graphene. *J. Comput. Phys.*, 379:403–420, 2019.
- [26] F. D. M. Haldane and S. Raghu. Possible realization of directional optical waveguides in photonic crystals with broken time-reversal symmetry. *Phys. Rev. Lett.*, 100(1):013904, 2008.
- [27] M. Z. Hasan and C. L. Kane. Topological insulators. *Rev. Mod. Phys.*, 82(4):3045–3067, 2010.
- [28] P. Hu, L. Hong, and Y. Zhu. Linear and nonlinear electromagnetic waves in modulated honeycomb media. *Stud. Appl. Math.*, 144(1):18–45, 2020.
- [29] R. Keller, J. Marzuola, B. Osting, and M. I. Weinstein. Spectral band degeneracies of $\frac{\pi}{2}$ -rotationally invariant periodic Schrödinger operators. *Multiscale Model. Simul.*, 16(4):1684–1731, 2018.
- [30] J. P. Lee-Thorp, M. I. Weinstein, and Y. Zhu. Elliptic operators with honeycomb symmetry: Dirac points, edge states and applications to photonic graphene. *Arch. Ration. Mech. Anal.*, 232(1):1–63, 2019.
- [31] J. Lin and H. Zhang. Mathematical theory for topological photonic materials in one dimension. *arXiv preprint arXiv:2101.05966*, 2021.
- [32] L. Lu, J. D. Joannopoulos, and M. Soljačić. Topological photonics. *Nature photonics*, 8(11):821, 2014.
- [33] T. Ma, A. B. Khanikaev, S. H. Mousavi, and G. Shvets. Guiding electromagnetic waves around sharp corners: topologically protected photonic transport in metawaveguides. *Physical Review Letters*, 114(12):127401, 2015.
- [34] S. H. Mousavi, A. B. Khanikaev, and Z. Wang. Topologically protected elastic waves in phononic metamaterials. *Nature communications*, 6(1):1–7, 2015.
- [35] A. H. C. Neto, F. Guinea, N. M. R. Peres, K. S. Novoselov, and A. K. Geim. The electronic properties of graphene. *Reviews of Modern Physics*, 81(1):109, 2009.
- [36] K. S. Novoselov, A. K. Geim, S. V. Morozov, D. Jiang, M. I. Katsnelson, I. V. Grigorieva, S. V. Dubonos, and A. A. Firsov. Two-dimensional gas of massless Dirac fermions in graphene. *Nature*, 438(7065):197–200, 2005.
- [37] S. Raghu and F. D. M. Haldane. Analogs of quantum-Hall-effect edge states in photonic crystals. *Phys. Rev. A*, 78(3):033834, 2008.
- [38] M. C. Rechtsman, J. M. Zeuner, Y. Plotnik, Y. Lumer, D. Podolsky, F. Dreisow, S. Nolte, M. Segev, and A. Szameit. Photonic Floquet topological insulators. *Nature*, 496(7444):196–200, 2013.
- [39] R. Süsstrunk and S. D. Huber. Observation of phononic helical edge states in a mechanical topological insulator. *Science*, 349(6243):47–50, 2015.
- [40] G. C. Thiang. Edge-following topological states. *Journal of Geometry and Physics*, 156:103796, 2020.
- [41] E. Witten. Three lectures on topological phases of matter. *La Rivista del Nuovo Cimento*, 39(7):313–370, 2016.
- [42] S. Wu, Y. Wu, and J. Mei. Topological helical edge states in water waves over a topographical bottom. *New Journal of Physics*, 20(2):023051, 2018.
- [43] P. Xie and Y. Zhu. Wave packet dynamics in slowly modulated photonic graphene. *J. Differential Equations*, 267(10):5775–5808, 2019.

- [44] P. Xie and Y. Zhu. Wave packets in the fractional nonlinear Schrödinger equation with a honeycomb potential. *Multiscale Model. Simul.*, 19(2):951–979, 2021.

YAU MATHEMATICAL SCIENCES CENTER, TSINGHUA UNIVERSITY, BEIJING 100084 AND YANQI LAKE BEIJING INSTITUTE OF MATHEMATICAL SCIENCES AND APPLICATIONS, BEIJING 101408, CHINA.
Email address: hpp1681@gmail.com

DEPARTMENT OF MATHEMATICS, THE HONG KONG UNIVERSITY OF SCIENCE AND TECHNOLOGY, CLEAR WATER BAY, KOWLOON, HONG KONG SAR.
Email address: mapengxie@ust.hk

YAU MATHEMATICAL SCIENCES CENTER, TSINGHUA UNIVERSITY, BEIJING 100084 AND YANQI LAKE BEIJING INSTITUTE OF MATHEMATICAL SCIENCES AND APPLICATIONS, BEIJING 101408, CHINA.
Email address: yizhu@tsinghua.edu.cn